Nano Energy 96 (2022) 107137

Contents lists available at ScienceDirect

Nano Energy

journal homepage: www.elsevier.com/locate/nanoen

Skin-inspired textile-based tactile sensors enable multifunctional sensing of wearables and soft robots☆

Yaokun Pang [a], Xianchen Xu [a], Shoue Chen [a], Yuhui Fang [c], Xiaodong Shi [b], Yiming Deng [b], Zhong-Lin Wang [d], Changyong Cao [a,*]

[a] Laboratory for Soft Machines & Electronics, Department of Mechanical and Aerospace Engineering, Case Western Reserve University, Cleveland, OH 44106, USA
[b] Department of Electrical & Computer Engineering, Michigan State University, East Lansing, MI 48824, USA
[c] 4D Maker LLC, Okemos, MI 48864, USA
[d] School of Materials Science & Engineering, Georgia Institute of Technology, Atlanta, GA 30332, USA

ARTICLE INFO

Keywords:
Multifunctional sensing
Skin-inspired
Tactile sensors
Textile sensor
Soft robots
Personalized healthcare
Wearables

ABSTRACT

Multifunctional tactile sensors that can mimic the sensory capabilities of human skin to perceive various external static and dynamic stimuli are essential to interact with the environment and humans for wearable electronics and soft intelligent robotics. Here, inspired by human skin, we report a textile-based tactile sensor capable of multifunctional sensing for personalized healthcare monitoring and soft robotic control. The tactile sensor consists of a triboelectric nanogenerator sensing layer to mimic the function of fast adapting (FA) mechanoreceptors and a piezoresistive sensing layer to achieve the functionality of slow adapting (SA) mechanoreceptors. The tactile sensor has been demonstrated to be able to recognize voice and monitor physiological signals and human motions in a real-time manner. Combined with a machine learning framework, the tactile sensor is able to percept surface textures and material types with high accuracy. It is also demonstrated as an effective human-machine interface for the control of assistive robotics.

1. Introduction

Multifunctional tactile perception is of paramount importance to achieve environment awareness and human-machine interactions in sophisticated applications of smart wearables and intelligent robots [1–8]. Over the past decade, inspired by human skin, various tactile sensors and artificial electronic skins (E-skins) have been proposed for precise and rapid sensing use based on different technologies, including piezoresistive [9], capacitive [10], electret [11], magnetic [12], triboelectric [13], etc. Furthermore, multiple sensors are integrated into a sensing network or array to enable multisensory functionality of the devices [7,14–16]. Although significant progress has been made in the development of tactile sensors and E-skins, some critical issues still need to be addressed urgently [14,16–20]. For example, most existing tactile sensors are designed based on a single sensing mechanism that cannot percept sufficient information and respond to complex stimuli [21]. The integration of multiple sensors remains very challenging, usually requiring the design of complicated structures and fabrication processes and may suffer from mutual interference in multiple stimuli perceptions [21–23]. In addition, polymer substrates such as polydimethylsiloxane (PDMS), polyethylene terephthalate (PET), and polyimide, are widely utilized for tactile sensors, resulting in poor air permeability and discomfort feeling for wearables [24]. Compared with polymers, textile is mechanically robust, soft, breathable, and comfortable to human skin, and an ideal material for wearable electronics [25]. However, due to the challenges in surface and interface integration, textile-based tactile sensors that can mimic the functions of mechanoreceptors are still lacking. Therefore, it is essential to develop new tactile sensors with excellent sensing performance and a simple fabrication process.

This article reports a textile-based tactile sensor for multifunctional sensing applications in health monitoring and soft robotics (Fig. 1). Inspired by the fingertip skin, we rationally design the tactile sensor with two sensing layers (Fig. 1A and B): a piezoresistive layer for mimicking the SA mechanoreceptor and a triboelectric layer with

☆ Prof Zhong Lin Wang, an author on this paper, is the Editor-in-Chief of Nano Energy, but he had no involvement in the peer review process used to assess this work submitted to Nano Energy. This paper was assessed, and the corresponding peer review managed by Dr Xia Cao, also an Associate Editor in Nano Energy.

* Correspondence to: Laboratory for Soft Machines & Electronics (SME), Department of Mechanical and Aerospace Engineering, Case Western Reserve University (CWRU), Cleveland, OH 44106, USA.
E-mail address: ccao@case.edu (C. Cao).

https://doi.org/10.1016/j.nanoen.2022.107137
Received 2 January 2022; Received in revised form 6 March 2022; Accepted 9 March 2022
Available online 15 March 2022
2211-2855/© 2022 Elsevier Ltd. All rights reserved.

fingerprint-inspired microlines for mimicking FA mechanoreceptor. This tactile sensor has the ability to perceive complex and combined mechanical stimuli, owing to its delicate fingerprint patterns and effective sensory receptors (Fig. 1C). With cotton fabric as the substrate material, the as-developed tactile sensors can easily conform to different body parts for health monitoring or complex surfaces of soft robotics for intelligent perceptions. The tactile sensors are demonstrated as wearable devices to monitor the voice, physiological signals, and joint motions of humans (Fig. 1D). Moreover, we develop a machine learning (ML)-based framework to integrate it with our tactile sensors for texture perception and material recognition. Finally, we demonstrate the use of the tactile sensor as a human-machine interface for assistive robotic control. This technology may significantly advance the development of wearable sensing devices and soft robotics.

2. Results

2.1. Design and fabrication of skin-inspired tactile sensors

Human skin has four types of mechanoreceptors that are distributed over different regions of human skin to perceive static and dynamic mechanical stimuli [2,26]. As shown in Fig. 1A, the two slow adapting mechanoreceptors (SA-I and SA-II) of fingertip skin can sensitively respond to low-frequency stimuli and produce a sustained signal to describe the static properties of a sustained stimulus [27,28]. In contrast, the two fast adapting mechanoreceptors (FA-I and FA-II) can detect dynamic pressure or vibrations [29,30], which is essential for texture discrimination and slip detection [31–33]. Novel tactile sensors that can mimic the SA and FA mechanoreceptors are highly desired for humanoid robots, intelligent prostheses, and wearable health monitoring devices [33,34].

To achieve the required functionality, we design the textile-based tactile sensor by integrating a piezoresistive sensor for mimicking the SA mechanoreceptor and a triboelectric sensor with fingerprint-inspired microlines for mimicking FA mechanoreceptor (Fig. 1B). The tactile sensor consists of a Cu-coated textile electrode layer, a carbon nanotube (CNT) coated piezoresistive sensing layer, a medical textile layer, and a top triboelectric layer. Cotton fabrics are utilized as the substrate material since they are soft, breathable, and comfortable to human skin [25,35,36]. Two electrodes with interdigitated configurations are fabricated via brush coating Cu ink on the cotton fabrics. The CNT-coated piezoresistive textile layer is fabricated by a low-cost and simple dip-coating method, stacking on top of the interdigitated electrodes [27,37]. Fig. S1a shows the scanning electron microscopy (SEM) image of the CNT-coated textile, indicating that the CNTs are uniformly covered on the surfaces of textile fibers. To encapsulate the electrodes, a biocompatible medical textile tape is bonded on the top of the CNT-coated textile to ensure a conformal contact between the CNT-coated textile and the electrodes and prevent mutual interference between the two different sensing layers.

Different from the previous fingerprint-like patterns fabricated with lithography methods, we utilize a facile approach to assemble a single-electrode triboelectric nanogenerator-based sensor by stitching structured core-shell (Teflon- steel) yarns (diameter ~ 300 μm, Fig. S1B) onto the cotton textile. The steel fiber core works as the conductive electrode while the Teflon shell layer serves as the dielectric material for triboelectrification because compared with other triboelectric materials such as PDMS and PET, Teflon exhibits a stronger ability of electron attraction and good mechanical strength. The details for the fabrication process are presented in Materials and Methods and Fig. S2. Similar to the

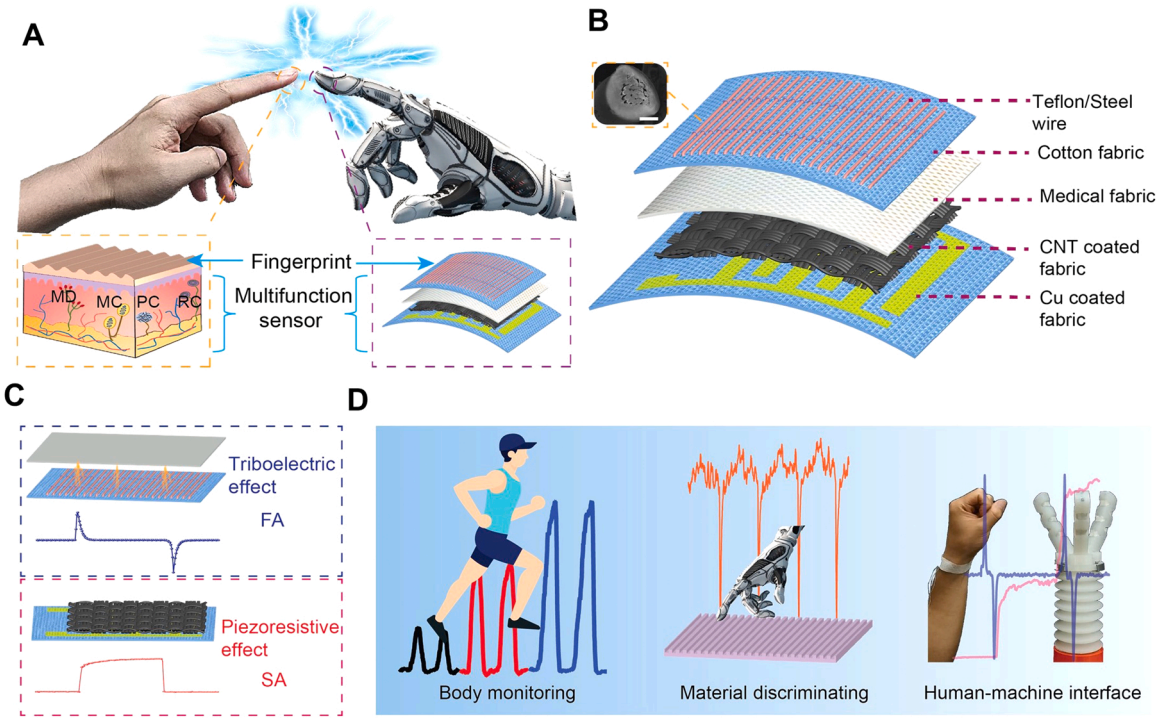

Fig. 1. Skin-inspired, self-powered, textile tactile sensors for multifunctional sensing in wearables and soft robotics. (A) Schematic of the skin-inspired all-textile tactile sensors capable of multifunctional tactile sensing. The basic structure of human skin versus all-textile tactile sensors (bottom); human skin has slow-adapting (SA) mechanoreceptors [Merkel (MD) and Ruffini corpuscles (RE)] for static stimuli, fast-adapting (FA) mechanoreceptors [Meissner (MC) and Pacinian corpuscles (PC)] for dynamic stimuli. (B) Detailed structure of the textile tactile sensors. (C) Schematics and representative output signals of the triboelectric sensor layer (top) and piezoresistive sensor layer (bottom) when subjected to pressure force. The triboelectric sensor can generate instantaneous pulse voltage signals at the moments of touching and separation with external dynamic stimuli as FA mechanoreceptors in human skin. The piezoelectric sensor has a similar function with the SA mechanoreceptors for detecting static or slowly varying stimuli. (D) Multifunctional applications of the textile sensors in health monitoring, material discriminating, and human-machine interface.

FA mechanoreceptor of skin, the triboelectric sensing layer generates a pulse electrical signal only at the moment of contact and separation with a mechanical stimulus. On the contrary, the piezoresistive sensing layer produces a maintained electrical signal during sustained indentation like the SA mechanoreceptor (Fig. 1C). Based on the synergistic effect of the triboelectric sensor and the piezoelectric sensor, our tactile sensor has the ability to detect complex physical stimuli such as human body motion, material discrimination, and work as a human-machine interface for the control of soft robotics (Fig. 1D).

2.2. Characterization of the piezoresistive sensing layer

Fig. 2 A illustrates the sensing mechanism of the proposed piezoresistive sensor layer. Different from a bulk rigid planar metal, the CNT-coated textile and the Cu-coated textile electrode layer have porous structures and rough surfaces. The contact area between the CNT-coated textile and the bottom electrodes changes as the applied external pressure varies. As shown in Fig. 2B, when the external pressure is applied onto the sensor surface, the porous structures deform, leading to the approaching and/or contact between the CNT-coated textile and the interdigital electrodes. This deformation generates a larger contact area and more conductive pathways between CNTs and Cu electrodes, leading to a significant increase of the current under an applied voltage. Once unloading, the CNT-coated textile and the bottom Cu electrode textile restore to their original states, resulting in the reduction of conductive pathways and thereby the decrease of the current.

We build an electrical signal testing platform to measure the sensing performance of the textile sensor devices (Fig. S3). As shown in Fig. 2C, the current-voltage (I-V) curves of the piezoresistive sensor exhibit excellent linear relationships under a specific static pressure loading, indicating that the CNT-coated textile and the Cu electrode textile form ohmic contacts. It is also demonstrated that the piezoresistive sensor exhibits high sensitivity and reliability for a wide range of applied pressure. We also observe that the slope of the I-V curve significantly increases with the applied pressure, indicating that the electrical resistance of the sensor device reduces continuously, which is consistent with the underlying sensing mechanism.

To facilitate the characterization of the performance of the piezoresistive sensor, we define the sensitivity (S) as $S = (\Delta I/I_0)/\Delta P$, where ΔI is the current change before and after applying pressure, I_0 is the initial current without pressure applied, and ΔP represents the applied pressure change. Fig. 2D shows the relative current change ($\Delta I/I_0$) as the applied pressure increases from 0 to 35 kPa. It is found that the curve can be divided into two segments with different slopes, corresponding to two different sensitivities. In the low-pressure region (0–11 kPa), the sensitivity of the sensor is 11.2/kPa while in the high-pressure region

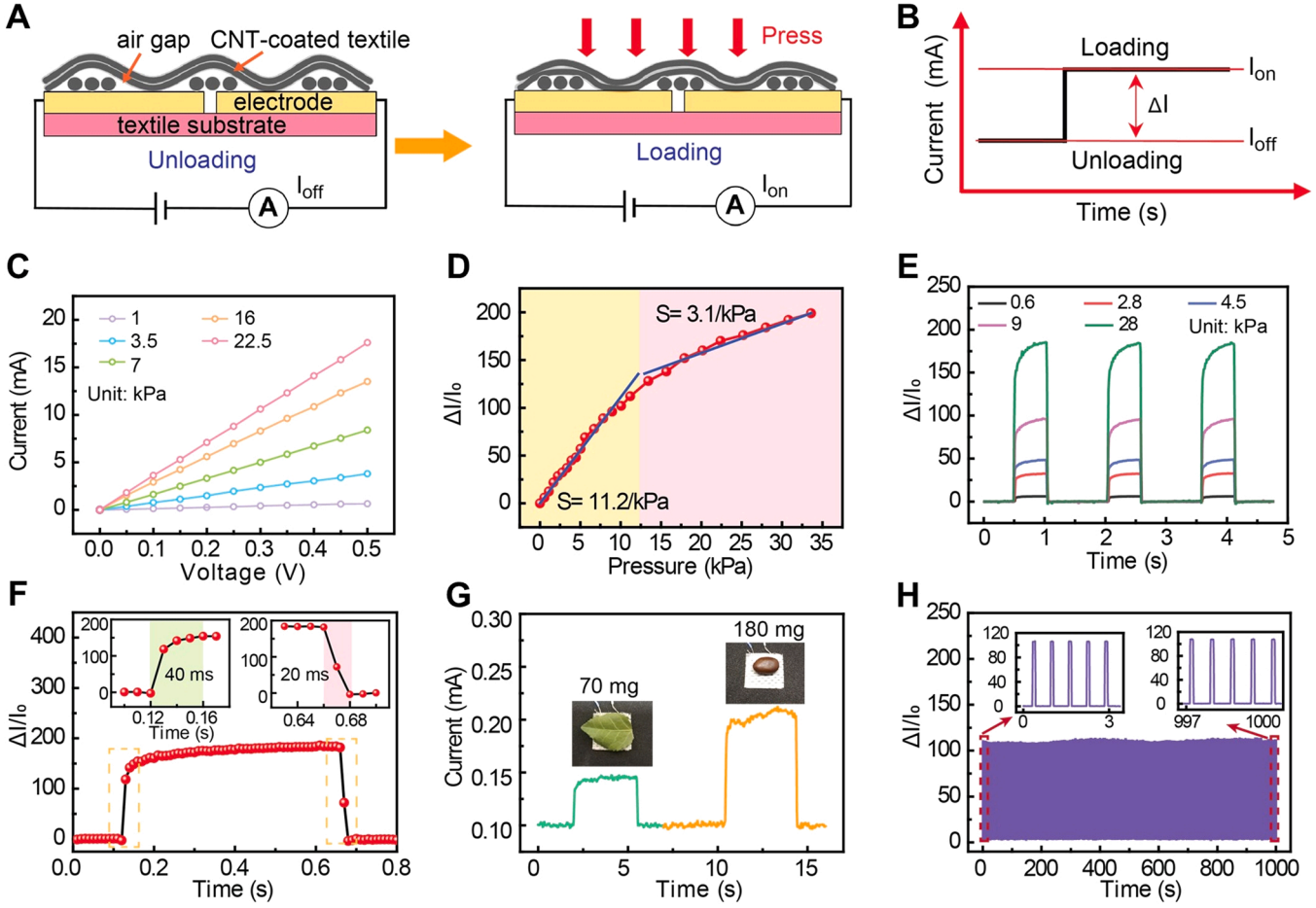

Fig. 2. Characterization of the piezoresistive sensing layer in the textile-based tactile sensor. (A) Schematic illustration of the working mechanism of the textile-based piezoresistive sensor layer. (B) Current responses of the tactile sensor under loading and unloading conditions. (C) I-V curves of the tactile sensor under different applied pressures varying from 1 kPa to 22.5 kPa. (D) Pressure sensitivity of the tactile sensor measured with different applied pressures. The pressure sensitivity ($S = (\Delta I/I_0)/\Delta P$) is estimated as 11.2 kPa^{-1} in the range of 0.5 kPa to 11 kPa and 3.1 kPa^{-1} in the range of 13.5 kPa to 33.5 kPa. (E) Real-time measurements of the relative current change by the tactile sensor under three cyclic loadings/unloading at different pressure levels. (F) The response time (40 ms) and recovery time (20 ms) of the tactile sensor in operations. (G) The current response curves of the sensor when loaded with a plant leaf (70 mg) and a seed (180 mg). The insets are the optical images of the leave and the seed in testing. (H) Reliability and stability tests of the textile sensor under the conditions of loading/unloading pressure of 10 kPa for 1500 cycles.

(13.5–33.5 kPa), the sensitivity is around 3.1/kPa. Fig. 2E shows the real-time measurement of the relative current change under cyclic loadings with different pressure magnitudes. All the measured current changes are varying with the applied pressures repeatedly, demonstrating its robustness and reliability. The measured response time for the tactile sensor is ~40 ms while the measured recovery time in sensing is ~20 ms (Fig. 2F). The sensitivity of the tactile sensor is excellent, and it can detect the small changes induced by loading–unloading a plant leaf (70 mg) and a seed (180 mg) (Fig. 2G). Moreover, the piezoresistive sensor exhibits excellent reproducibility and durability (Fig. 2H). It is demonstrated that for more than 1500 cycles of repeated loading-unloading of a pressure of 10 kPa, there is no obvious change of the relative current signals.

Additionally, we demonstrate the tactile sensor can be used for monitoring various physiological signals and joint motions of wearers in a real-time manner when it is deployed at different body parts (Fig. 3A). For example, when the textile-based sensor is attached to the throat region of a volunteer, it can accurately sense the muscle movement at the throat region when speaking and thereby recognize the voice patterns (Fig. 3B, C, and S4). As shown in Fig. 3B, the sensor can recognize the different words spoken by the person in a sentence through the unique signal patterns detected through the different epidermis movements induced by laryngeal prominence. Furthermore, the sensor demonstrates good repeatability in recognizing the specific words in speaking (Fig. 3C). For example, when the volunteers say the same word "hello" repeatedly five times, it obtains nearly identical signal patterns of voice signals. Therefore, this sensor has the potential to be used for natural language-based human-machine interfaces and phonation rehabilitation exercises [38].

In personalized healthcare, vital physiological signals such as heart or pulse rate are valuable information for evaluating the medical conditions of patients with cardiovascular disease [39]. As a demonstration, we attach the textile sensor onto the wrist surface of a volunteer to monitor the pulse rate and pulse waveform in a real-time manner (Fig. 3D). Fig. 3E shows the pulse signals recorded for a period of 9 s, indicating a recorded pulse rate of ~68 beats/min, within the normal range of a healthy adult. Furthermore, from the recorded regular and repeated signal patterns, the sensor is able to distinguish the three characteristic peaks of a standard pulse waveform, i.e., "P" (percussion wave), "T" (tidal wave), and "D" (diastolic wave) [40,41], indicating the great potential of such sensors in biomedical applications.

We further demonstrate the textile sensor worked as a motion detector to record the current response under the bending-releasing cycles when mounted at the joints of the human body, such as elbow, wrist, knee, and ankle (Fig. 3A). If the piezoresistive sensor is directly attached on the elbow, the sensor is compressed as the elbow bends, causing an increase of conductive pathway and thereby a decrease of the conducting resistance and an increase of the current. When the bending angle decreases, the current signal becomes smaller (Fig. 3F). Similarly, the sensor is capable of accurately detecting the bending motions of the

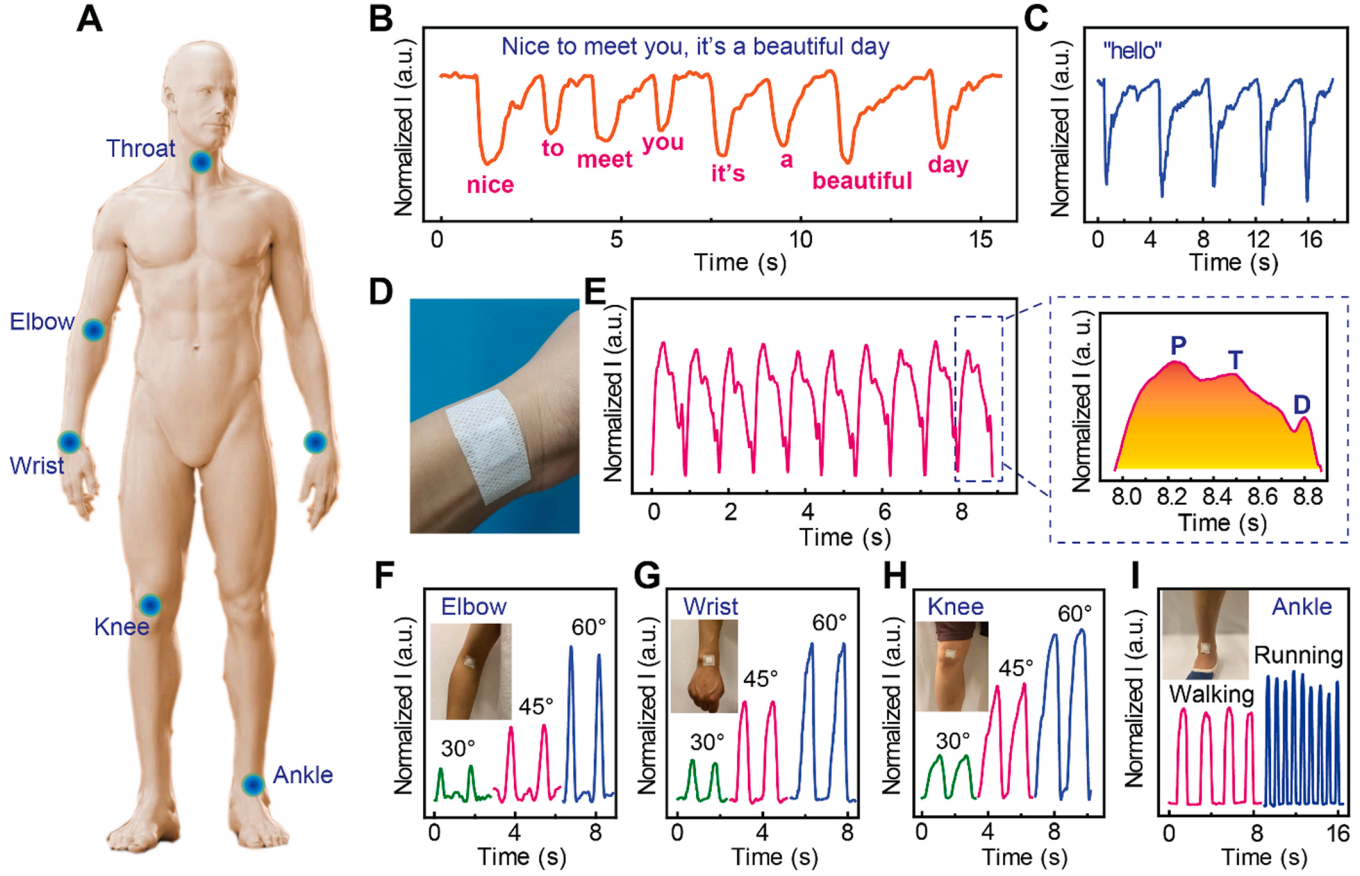

Fig. 3. Real-time monitoring of physiological signals and body motions using the textile-based tactile sensor. (A) Schematic illustration of a human body with the possible monitoring positions marked by blue color. (B) Real-time current signal measured by the tactile sensor when a volunteer wears the sensor in throat region and speaks "Nice to meet you, it's a beautiful day". Different words can be recorded and distinguished based on the unique signal patterns of pronunciation. (C) Real-time current signal responding to the words "hello" five times. It demonstrates excellent repeatability in voice recognition. (D) Photograph of the sensor device bonded on the wrist surface for detecting artery pulse pressure. (E) Real-time current signal responding to the artery pulse pressure. Each pulse waveform can clearly show the typical P-wave, T-wave, and D-wave. (F-H) Real-time current signals measured by the tactile sensors for the bending-releasing movement of (F) elbow, (G) wrist, (H) knee under different bending angles. (I) Real-time current signal measured by the tactile sensor attached on the ankle to detect human movement states: running and walking.

wrist and knee (Fig. 3G and H). Furthermore, we find that the sensor attached to the ankle joint can detect and discriminate human movement states. When the person is walking or running, the amplitude and frequency of human motion are quite different, which can be reflected through the induced current change in the sensor at different motion states (Fig. 3I). These results indicate that our sensor can be readily utilized for detecting kinematic signals and joint motions and should promising applications in the fields of personalized health monitoring, human-machine interface, athletic performance monitoring, and patient rehabilitation.

2.3. Characterization of the triboelectric sensing layer

Fig. 4 A illustrates the working mechanism of the triboelectric sensing layer for the tactile sensor which is essentially a single-electrode TENG based on the coupling effect of contact electrification and electrostatic induction. This design of the single-electrode mode is especially suitable for tactile sensing owing to its simple structure and design [42]. When an active object contacts the Teflon surface, negative triboelectric charges are gained by Teflon due to its stronger electron affinities while the active object becomes positive charged (Fig. S5). Once the active object separates from the Teflon surface, the potential difference between the two triboelectric layers will gradually increase, resulting in an instantaneous electron flow from the Cu electrode to the ground and generating an output voltage to the external load. When the two kinds of materials approach each other again, the electrons will flow back from the ground to the Cu electrode with a reversed output signal appearing. To test its sensing performance, we use an Ecoflex film (15 $\times$15 mm^2) as the contact material and a linear motor to provide repetitive contact-separation motions. Fig. 4b presents the output voltages of the TENG with pressures varying from 0 to 56 kPa. It is obvious that the output voltages have a nearly linear relationship with the applied pressure that is not larger than 22 kPa. The output voltage also depends on the touching frequency, and an increased frequency leads to a higher voltage, consistent with our previous studies [43,44] (Fig. 4C).

In addition, the unique working mechanism of the TENG-based sensor enables it to be able to sense different kinds of materials based on their inherent ability to lose/gain electrons. After the possible materials' properties are gathered, the proposed design and method can be extended for use in sorting more different materials [45]. As shown in Fig. S6, twelve kinds of materials are screened for demonstration in our experiments. The amplitude and polarity of the output voltage by the TENG sensing layer change with the different contacting materials. The insets in Fig. S6 illustrate the voltage signals in one cycle with the two contacting materials: polyethylene (bottom) and Ecoflex (top). Compared with Teflon used in our sensor fabrication, polyethylene (PE), Nylon, polylactic acid (PLA), Cu, polyethylene terephthalate (PET), natural latex, and polypropylene (PP) are tending to lose electrons when they are in contact with Teflon, resulting in a positive voltage signal. On the contrary, Kapton, polyvinyl chloride (PVC), polytetrafluoroethylene (PTFE), and fluorinated ethylene propylene (FEP) exhibit a stronger ability to gain electrons, resulting in a negative voltage signal. Through the comparison of the amplitude and polarity of the output voltage, we can use the tactile senor to identify the type of the contact materials, which may be useful for automatic object sorting and separation in recycling and fabrication processes.

The TENG-based sensing layer can also recognize the surface morphology or texture. In our design, the fabricated sensor is attached onto a semicylindrical micro stage and then scans over the sample surfaces that have parallel line textures (Fig. 4D). Different from the contact-separation working mode shown in Fig. 4A, for the surface morphology and texture recognition the TENG sensor works in a single-electrode-based sliding mode (Fig. S7). As the sensor slides on the sample surface at the velocity of 0.5 mm s^{-1}, the fingerprint-like steel/Teflon fiber contacts and separates with the ridges of the micropatterns, resulting in the corresponding variations of the voltage signals (Fig. 4E). The observed voltage signals decrease with the increasing wavelength of the periodic patterns at the same scanning speed. The voltage signals in the frequency domain obtained by Fast Fourier transform (FFT) can give the characteristic frequencies that agree with the spatial frequencies of the micropatterns (Fig. 4F). For a defined texture pattern, the number of voltage signals and the corresponding characteristic frequencies increase with the scanning speeds (0.3–1 mm s^{-1}) (Fig. S8).

For possible large-scale applications of dense sensor arrays, it is impossible to get identical devices and sensing data with the same quality in practical fabrications and operations, especially for low-resolution soft electronics. Therefore, we propose a machine learning (ML) based framework to analyze and classify the voltage signals obtained from the TENG sensors, aiming to achieve robust sensing capability in material recognition and surface texture detection. We select the artificial neural network (ANN) method to build the model, which consists of an input layer, three hidden layers, and an output layer (Fig. 4G). We use the LM training function and the nine different materials with different textures as the training data to minimize the ANN's MSE by adjusting the connection weights and bias (Fig. 4H). Performance and generalization of the ANNs are further tested using independent testing data for cross-validation. As shown in Fig. 4I, the training accuracy can reach up to 99.98%. More details on the training method and error analysis are in Materials and Methods and Supplementary note. Fig. 4J presents the confusion map of the machine learning outcome in predicting the materials from M1-M9, where the prediction accuracy is about 94.44%.

2.4. Demonstration and evaluation of the textile-based tactile sensor

Human skin can sense the material hardness in touching the objects. However, it is generally difficult for robotics to achieve that task using one single sensor. Here, we further demonstrate our tactile sensor for sensing the relative hardness of objects through a simple operation mechanism (Fig. 5A). The latex balloons inflated by different air pressures are used to represent the relative hardness of the touching objects. When the tactile sensor contacts or separates with the touching objects (balloons), the TENG sensing layer generates instantaneous negative and positive voltage signals due to the contact electrification, respectively (Fig. 5B, top). In comparison, the pressing and releasing motions are detected by the recorded signals from the piezoresistive sensing layer (Fig. 5B, bottom). The up-hill side and down-hill side of a current curve represented the pressing and releasing state, and the current value increases with the hardness of the object (balloon) because a larger hardness results in a large pressure applied to the sensor. Such a sensing capability enables the use of the new tactile sensors in advanced manipulations such as fruit picking to avoid potential physical damage.

We finally demonstrate the tactile sensors as an effective human-machine interface to control a soft robotic manipulator (Movie S1). As shown in Fig. 5C, the whole system consists of a soft robotic gripper, a soft arm, a signal processing and transmitting module, and a tactile sensor. The control signals performed by the human (e.g., wrist bending and sensor pressing) are first processed and sent to the analog ports of the Arduino board in the circuit. Then, the analog-to-digital converter (ADC) converts the analog signals into digital values and transmitted them to a control board [46]. After that, the received signals will be compared with the pre-defined thresholds to determine whether and how to activate the DC motors to actuate the soft manipulator. Fig. 5D and E illustrate the real-time signals recorded in the manipulation and the corresponding motion states of the soft robotic manipulator. In the original state (I), the tactile sensor is attached on the wrist and the soft arm is vertically standing on a table. When the human wrist bends (II), a continuous current signal output is detected due to the flexion of the wrist, and thereby the soft arm bends to the right side with a small bending angle. In state III, the wrist ends to a larger angle, the current signal increases further, leading to a larger bending angle of the soft robotic arm. When the tactile sensor is pressed slightly using a finger

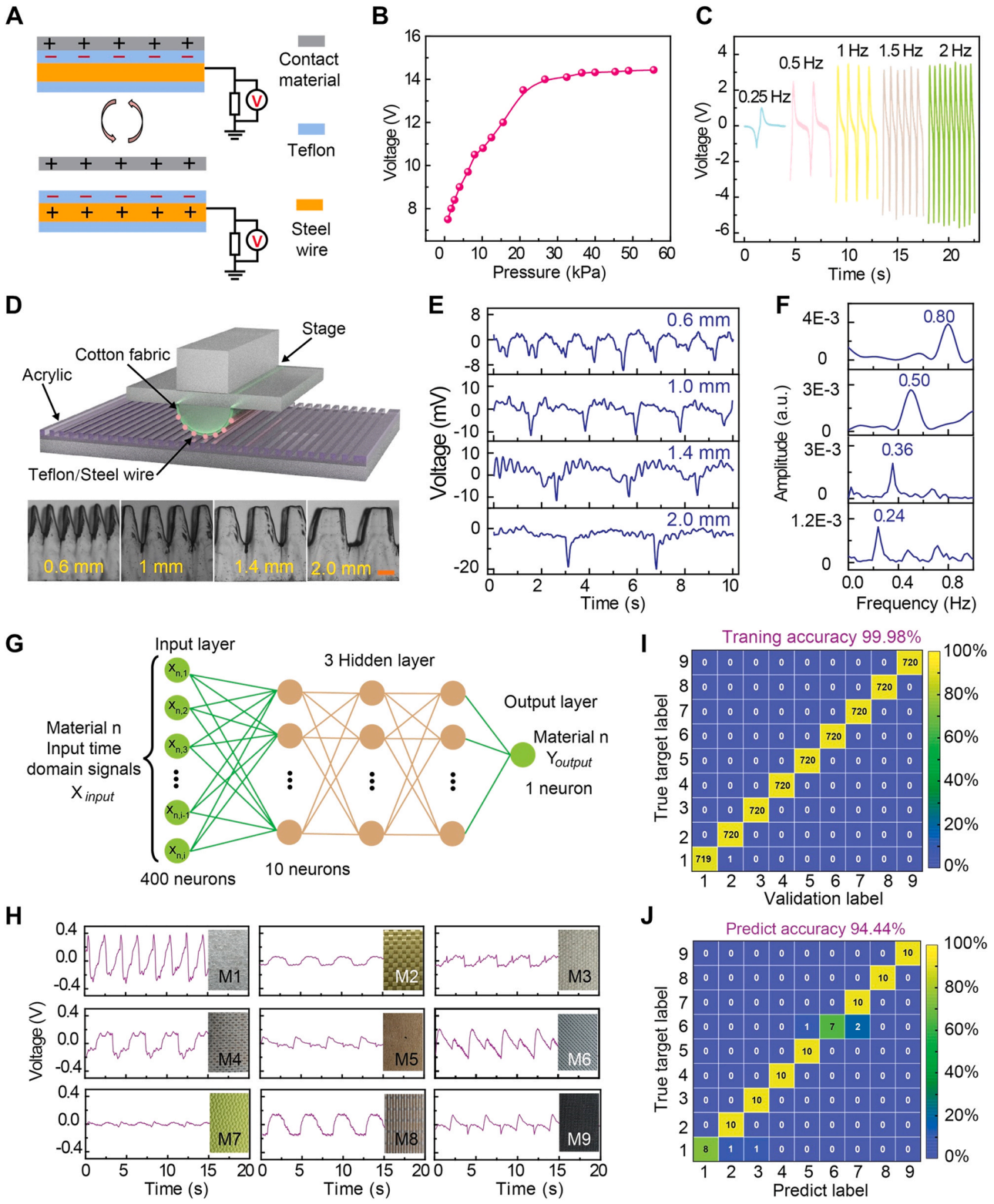

Fig. 4. Characterization and demonstration of the triboelectric sensing layer in tactile sensor for texture perception and material discrimination. (A) Working principle of the triboelectric sensor layer. (B) Variations of the output voltage of the triboelectric sensor as a function of loading force. (C) Output voltages of the triboelectric sensor under different frequencies (0.25–2 Hz). (D) Schematic illustration of the texture perception through a sliding touch by the tactile sensor. The triboelectric sensor is attached to a semicylindrical stage and scanned over a surface with parallel line patterns. The bottom is the photographs of the micropatterned surfaces fabricated by a laser cutter (scale bar: 500 μm). (E) The voltage signals obtained by the triboelectric sensor when it is scanned over different micropatterns. (F) Fast Fourier transform (FFT) spectra of time-dependent voltage signals in (E), showing the spatial frequency of the micropatterns. (G) Schematic diagram of the artificial neural network (ANN) used for material identification. The ANN consists of an input layer, 3 hidden layers, and an output layer where all the neurons between each layer are fully connected to each other. (H) The material list with real material images and its corresponding time-domain signal for training. (I) The confusion map for classifying the materials from M1∼M9. (J) The confusion map for classifying the materials in predicting materials from M1∼M9.

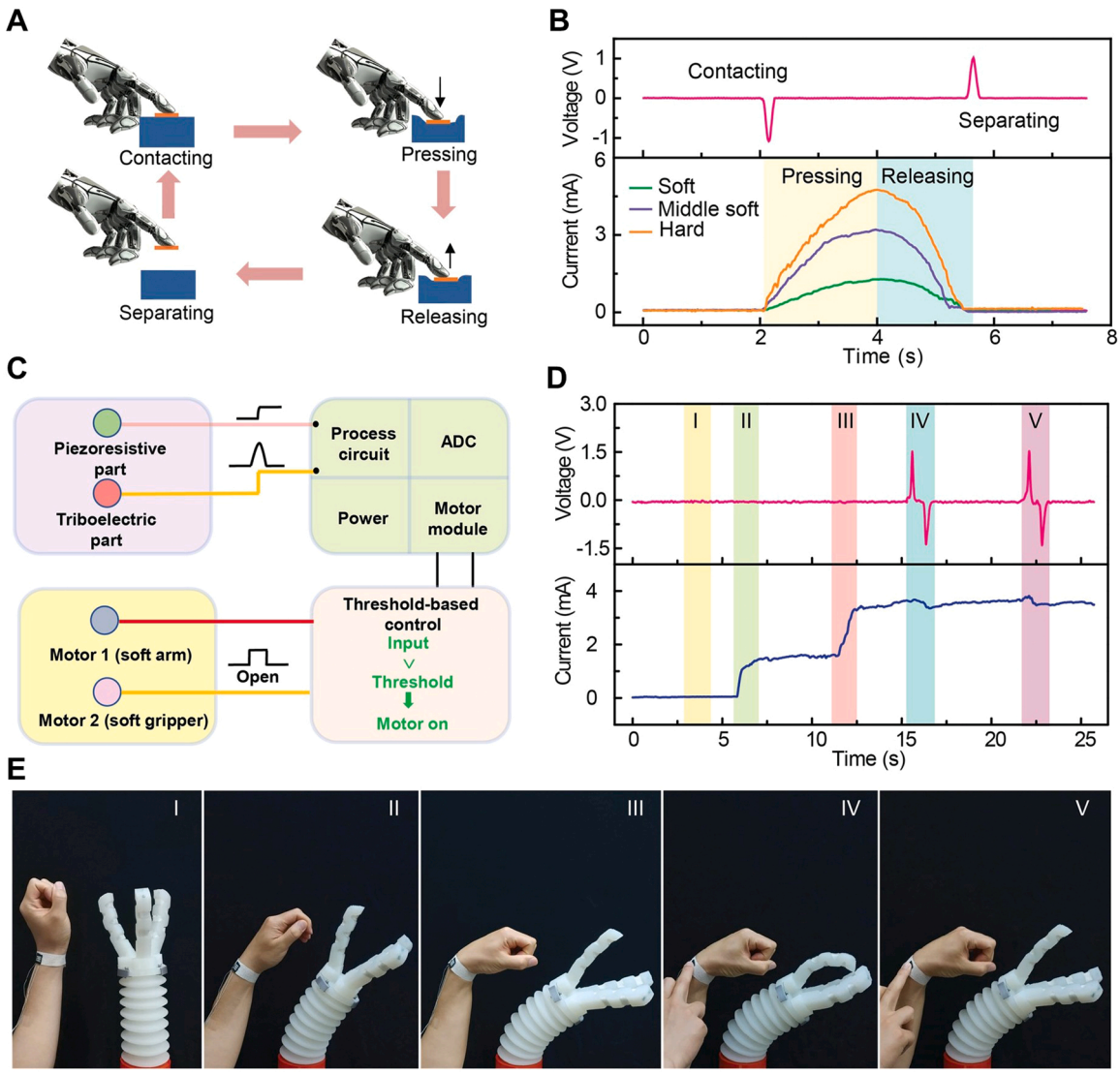

Fig. 5. Demonstration of the textile based tactile sensor for resolving complex stimuli and controlling soft robots. (A) Schematic of the detection of the touching objects using a soft robotic hand equipped with our tactile sensors on its fingers. (B) Real-time signals of the tactile sensors induced in the touching process with an object. The triboelectric layer generates instantaneous pulse voltage signals once it contacts or separates with an object. The current signal can be used to identify the relative hardness of the touched object in the pressing and releasing processes. (C) Schematic diagram of the remote soft robotic control system using our tactile sensor as a human-machine interface (ADC: analog-digital converter). (D) Real-time signals of the tactile sensors generated at five different operation states: three bending angles of the wrist and switching on and off by finger. (E) Photographs of the soft robotic manipulator and human arm under different control commands controlled by the sensor, which are compounding to the control signals shown in (D).

(IV), the induced voltage signal in the TENG sensing layer actuates the grasping operation of the soft gripper. When pressing the sensor again, the soft gripper can open its fingers to its initial releasing state (V). It is expected that our textile tactile sensor can be used as a useful human-machine interface for controlling soft robots to complete more complex tasks in the future.

Supplementary material related to this article can be found online at doi:10.1016/j.nanoen.2022.107137.

3. Conclusion

We have reported a textile-based multifunctional tactile sensor that can mimic the SA and FA mechanoreceptors of human skins through the integration of triboelectric and piezoresistive sensors. The piezoresistive part utilizes CNT-textile as piezoresistive materials shows a high sensitivity of 11.2 kPa^{-1}, short response time (<40 ms), and good stability. The TENG-based sensing part fabricated by stitching Teflon-steel yarns onto a cotton textile successfully achieves the functionality of FA mechanoreceptor. With these superior performances of the two components, our textile tactile sensing layer has been demonstrated to monitor various human physiological signals and human joint motions in a real-time manner. We have also explored its potential applications in material identification and texture recognition with the assistance of an ML-based approach. Moreover, the device also enables the detection of complex stimuli and controlling of soft robotics as a wearable human-machine interface. It is expected that this study will provide a new strategy for developing novel multifunctional sensors with promise in smart textiles, wearable electronics, and robotics.

4. Materials and methods

4.1. Fabrication of textile sensors

A 10 × 10 mm^2 cotton textile was dipped into a CNT solution for 10 s and dried on a hot plate for 10 min at 70 ℃ to evaporate the solvent. This dip-coating and drying process was repeated for about 10 cycles

and the color of the textile changed from white to black. Then, cotton textile was covered by a tape tightly as a mask layer. An interdigital electrode pattern was designed by AutoCAD and then written onto the surface of the tape without damaging the textile substrate by using a computer-controlled commercial laser cutter system (Glowforge plus). Cu ink was coated on the surface of the cotton textile with a mask by a brush coating method and dried in a vacuum oven for about 1 h. Commercial Teflon/steel fiber was stitched onto a cotton textile to assemble a signal electrode triboelectric sensor. Finally, the electrode layer, CNT-coated piezoresistive layer, medical textile tape, and triboelectric layer were integrated together.

4.2. Morphological characterization

The microstructures of the CNT-coated textile and the stain-Teflon fiber were characterized using a Zeiss Auriga Cross Beam. The photographs of the micropatterns were characterized using optical microscopy (Olympus SZX12).

4.3. Measurements of the sensing performance

The current and voltage signals were measured by a current preamplifier (Keithley 6514 System Electrometer) and a digital storage oscilloscope (GDS-2202). A linear motor (LinMot MBT-37 120) was employed to apply different pressures onto the device. The software LabVIEW was programmed to acquire real-time control and data extraction. A force gauge (ZP-100 N) was used to detect applied pressure.

4.4. Modeling of the sensing mechanism

The potential distribution of the TENG sensor was simulated by using the software package COMSOL. For simplicity's purpose, the TENG sensor is treated as a parallel-plate capacitor in the established model, where the Teflon plate with steel electrode was placed parallelly with the PE plate. The triboelectric charge density on the inner surface of the Teflon plate was assigned as 1 $\mu C/m^2$.

4.5. Machine learning for material recognition

All the neurons between every layer are fully connected by each other and the input time-domain signals of each material have $i = 400$ neurons, where $n \in [1, 2, \ldots, N]$ and N is the types of materials that have been used to train the network and output layer are their list number of materials types from 1 to N. We used the 'fitnet' function in the software package MATLAB to develop fully connected propagation ANNs, which has an input, output, and one or more hidden layers designed for function approximation and nonlinear regression. Compared to the CNN net, we use the time domain signal other than material figures as input, and the material label is used as a regression target. In this process, the input time-domain data of N types of materials are reorganized to N types of 400×720 matrix. For each input vector and output layer, we have 400 neurons and 1 neuron, respectively. The training function can be regarded as $f(X_{input})=Y_{output}$. The different numbers of neurons in hidden layers are used to optimize the training accuracy of ANN. In our analysis, ten neurons in the three hidden layers are chosen to predict the material types from the tested signals.

CRediT authorship contribution statement

C.C. and Y.P. conceived the project and designed the experiments. **Y.P.** performed the experiments. **X.X.** performed the machine learning based analysis. **S.C.** assisted the experiments and demonstration. **Y.P., Y.F., S.C. and X.X.** analyzed the data. **C.C., Z.-L.W. and Y. D.** supervised the project. **Y.P. and C.C.** wrote the manuscript and all authors provided feedback and revision comments.

Declaration of Competing Interest

The authors declare that they have no known competing financial interests or personal relationships that could have appeared to influence the work reported in this paper.

Acknowledgements

This work was partially supported by the National Science Foundation (ECCS-2024649) and U.S. Department of Transportation (693JK32050003CAAP) and Case Western Reserve University.

Appendix A. Supporting information

Supplementary data associated with this article can be found in the online version at doi:10.1016/j.nanoen.2022.107137.

References

[1] Y.C. Lai, J. Deng, R. Liu, Y.C. Hsiao, S.L. Zhang, W. Peng, H.M. Wu, X. Wang, Z. L. Wang, Actively perceiving and responsive soft robots enabled by self-powered, highly extensible, and highly sensitive triboelectric proximity-and pressure-sensing skins, Adv. Mater. 30 (2018), 1801114.
[2] A. Chortos, J. Liu, Z. Bao, Pursuing prosthetic electronic skin, Nat. Mater. 15 (2016) 937–950.
[3] J. Park, M. Kim, Y. Lee, H.S. Lee, H. Ko, Fingertip skin–inspired microstructured ferroelectric skins discriminate static/dynamic pressure and temperature stimuli, Sci. Adv. 1 (2015), e1500661.
[4] S. Chun, W. Son, H. Kim, S.K. Lim, C. Pang, C. Choi, Self-powered pressure- and vibration-sensitive tactile sensors for learning technique-based neural finger skin, Nano Lett. 19 (2019) 3305–3312.
[5] X. Wu, J. Zhu, J.W. Evans, A.C. Arias, A single-mode, self-adapting, and self-powered mechanoreceptor based on a potentiometric–triboelectric hybridized sensing mechanism for resolving complex stimuli, Adv. Mater. 32 (2020), 2005970.
[6] Y. Lee, J. Park, A. Choe, S. Cho, J. Kim, H. Ko, Mimicking human and biological skins for multifunctional skin electronics, Adv. Funct. Mater. 30 (2019), 1904523.
[7] Q. Hua, J. Sun, H. Liu, R. Bao, R. Yu, J. Zhai, C. Pan, Z.L. Wang, Skin-inspired highly stretchable and conformable matrix networks for multifunctional sensing, Nat. Commun. 9 (2018) 244.
[8] T.Q. Trung, N.-E. Lee, Flexible and stretchable physical sensor integrated platforms for wearable human-activity monitoringand personal healthcare, Adv. Mater. 28 (2016) 4338–4372.
[9] J. Kim, M. Lee, H.J. Shim, R. Ghaffari, H.R. Cho, D. Son, Y.H. Jung, M. Soh, C. Choi, S. Jung, K. Chu, D. Jeon, S.T. Lee, J.H. Kim, S.H. Choi, T. Hyeon, D.H. Kim, Stretchable silicon nanoribbon electronics for skin prosthesis, Nat. Commun. 5 (2014) 1–11.
[10] C.G. Núñez, W.T. Navaraj, E.O. Polat, R. Dahiya, Energy-autonomous, flexible, and transparent tactile skin, Adv. Funct. Mater. 27 (2017), 1606287.
[11] S. Gong, J. Zhang, C. Wang, K. Ren, Z.L. Wang, A monocharged electret nanogenerator-based self-powered device for pressure and tactile sensor applications, Adv. Funct. Mater. 29 (2019), 1807618.
[12] X. Yu, Z. Xie, Y. Yu, J. Lee, A. Vazquez-Guardado, H. Luan, J. Ruban, X. Ning, A. Akhtar, D. Li, B. Ji, Y. Liu, R. Sun, J. Cao, Q. Huo, Y. Zhong, C. Lee, S. Kim, P. Gutruf, C. Zhang, Y. Xue, Q. Guo, A. Chempakasseril, P. Tian, W. Lu, J. Jeong, Y. Yu, J. Cornman, C. Tan, B. Kim, K. Lee, X. Feng, Y. Huang, J.A. Rogers, Skin-integrated wireless haptic interfaces for virtual and augmented reality, Nature 575 (2019) 473–479.
[13] Y. Cheng, D. Wu, S. Hao, Y. Jie, X. Cao, N. Wang, Z.L. Wang, Highly stretchable triboelectric tactile sensor for electronic skin, Nano Energy 64 (2019), 103907.
[14] G. Li, S. Liu, L. Wang, R. Zhu, Skin-inspired quadruple tactile sensors integrated on a robot hand enable object recognition, Sci. Robot. 5 (2020) eabc8134.
[15] Z. Huang, Y. Hao, Y. Li, H. Hu, C. Wang, A. Nomoto, T. Pan, Y. Gu, Y. Chen, T. Zhang, W. Li, Y. Lei, N. Kim, C. Wang, L. Zhang, J.W. Ward, A. Maralani, X. Li, M.F. Durstock, A. Pisano, Y. Lin, S. Xu, Three-dimensional integrated stretchable electronics, Nat. Electron. 1 (2018) 473–480.
[16] C.M. Boutry, M. Negre, M. Jorda, O. Vardoulis, A. Chortos, O. Khatib, Z. Bao, A hierarchically patterned, bioinspired e-skin able to detect the direction of applied pressure for robotics, Sci. Robot. 3 (2018).
[17] N. Bandari, J. Dargahi, M. Packirisamy, Tactile sensors for minimally invasive surgery: a review of the state-of-the-art, applications, and perspectives, IEEE Access 8 (2020) 7682–7708.
[18] K. Sim, Z. Rao, Z. Zou, F. Ershad, J. Lei, A. Thukral, J. Chen, Q.A. Huang, J. Xiao, C. Yu, Metal oxide semiconductor nanomembrane–based soft unnoticeable multifunctional electronics for wearable human-machine interfaces, Sci. Adv. 5 (2019) eaav9653.
[19] Y. Wu, Y. Liu, Y. Zhou, Q. Man, C. Hu, W. Asghar, F. Li, Z. Yu, J. Shang, G. Liu, M. Liao, R.W. Li, A skin-inspired tactile sensor for smart prosthetics, Sci. Robot. 3 (2018) eaat0429.

[20] S.Y. Kim, S. Park, H.W. Park, D.H. Park, Y. Jeong, D.H. Kim, Highly sensitive and multimodal all-carbon skin sensors capable of simultaneously detecting tactile and biological stimuli, Adv. Mater. 27 (2015) 4178–4185.
[21] J.C. Yang, J. Mun, S.Y. Kwon, S. Park, Z. Bao, S. Park, Electronic skin: recent progress and future prospects for skin-attachable devices for health monitoring, robotics, and prosthetics, Adv. Mater. 31 (2019), 1904765.
[22] Y. Lee, J.-H. Ahn, Biomimetic tactile sensors based on nanomaterials, ACS Nano 14 (2020) 1220–1226.
[23] D.H. Ho, Q. Sun, S.Y. Kim, J.T. Han, D.H. Kim, J.H. Cho, Stretchable and multimodal all graphene electronic skin, Adv. Mater. 28 (2016) 2601–2608.
[24] W. Fan, Q. He, K. Meng, X. Tan, Z. Zhou, G. Zhang, J. Yang, Z.L. Wang, Machine-knitted washable sensor array textile for precise epidermal physiological signal monitoring, Sci. Adv. 6 (2020) eaay2840.
[25] J. Shi, S. Liu, L. Zhang, B. Yang, L. Shu, Y. Yang, M. Ren, Y. Wang, J. Chen, W. Chen, Y. Chai, X. Tao, Smart textile-integrated microelectronic systems for wearable applications, Adv. Mater. 32 (2019), 1901958.
[26] P. Delmas, J. Hao, L. Rodat-Despoix, Molecular mechanisms of mechanotransduction in mammalian sensory neurons, Nat. Rev. Neurosci. 12 (2011) 139–153.
[27] S. Gong, W. Schwalb, Y. Wang, Y. Chen, Y. Tang, J. Si, B. Shirinzadeh, W. Cheng, A wearable and highly sensitive pressure sensor with ultrathin gold nanowires, Nat. Commun. 5 (2014) 3132.
[28] Y. Cao, T. Li, Y. Gu, H. Luo, S. Wang, T. Zhang, Fingerprint-inspired flexible tactile sensor for accurately discerning surface texture, Small 14 (2018), 1703902.
[29] H.L. Wang, S.Y. Kuang, H.Y. Li, Z.L. Wang, G. Zhu, Large-area integrated triboelectric sensor array for wireless static and dynamic pressure detection and mapping, Small 16 (2019), 1906352.
[30] X. Zhao, Z. Zhang, L. Xu, F. Gao, B. Zhao, T. Ouyang, Z. Kang, Q. Liao, Y. Zhang, Fingerprint-inspired electronic skin based on triboelectric nanogenerator for fine texture recognition, Nano Energy 85 (2021), 106001.
[31] A.I. Weber, H.P. Saal, J.D. Lieber, J.W. Cheng, L.R. Manfredi, J.F. Dammann, S. J. Bensmaia, Spatial and temporal codes mediate the tactile perception of natural textures, Proc. Natl. Acad. Sci. USA 110 (2013) 17107–17112.
[32] R.S. Johansson, J.R. Flanagan, Coding and use of tactile signals from the fingertips in object manipulation tasks, Nat. Rev. Neurosci. 10 (2009) 345–359.
[33] M. Wang, Y. Luo, T. Wang, C. Wan, L. Pan, S. Pan, K. He, A. Neo, X. Chen, Artificial skin perception, Adv. Mater. 33 (2020), 2003014.
[34] N. Salimi-Nezhad, M. Amiri, E. Falotico, C. Laschi, A digital hardware realization for spiking model of cutaneous mechanoreceptor, Front. Neurosci. 12 (2018) 322.
[35] W. Weng, P. Chen, S. He, X. Sun, H. Peng, Smart electronic textiles, Angew. Chem. Int. Ed. 55 (2016) 6140–6169.
[36] M. Liu, X. Pu, C. Jiang, T. Liu, X. Huang, L. Chen, C. Du, J. Sun, W. Hu, Z.L. Wang, Large-area all-textile pressure sensors for monitoring human motion and physiological signals, Adv. Mater. 29 (2017), 1703700.
[37] J. An, Y. Ma, M. He, J. Yan, C. Zhang, X. Li, P. Shen, S. Luo, Y. Gao, A wearable and highly sensitive textile-based pressure sensor with Ti3C2Tx nanosheets, Sens. Actuators A Phys. 311 (2020), 112081.
[38] X. Fang, J. Tan, Y. Gao, Y. Lu, F. Xuan, High-performance wearable strain sensors based on fragmented carbonized melamine sponges for human motion detection, Nanoscale 9 (2017) 17948–17956.
[39] Y. Khan, A.E. Ostfeld, C.M. Lochner, A. Pierre, A.C. Arias, Monitoring of vital signs with flexible and wearable medical devices, Adv. Mater. 28 (2016) 4373–4395.
[40] S. Chen, Y. Song, F. Xu, Flexible and highly sensitive resistive pressure sensor based on carbonized crepe paper with corrugated structure, ACS Appl. Mater. Interfaces 10 (2018) 34646–34654.
[41] X. Li, Y.J. Fan, H.Y. Li, J.W. Cao, Y.C. Xiao, Y. Wang, F. Liang, H.L. Wang, Y. Jiang, Z.L. Wang, G. Zhu, Ultracomfortable hierarchical nanonetwork for highly sensitive pressure sensor, ACS Nano 14 (2020) 9605–9612.
[42] Z.L. Wang, Triboelectric nanogenerators as new energy technology for self-powered systems and as active mechanical and chemical sensors, ACS Nano 7 (2013) 9533–9557.
[43] X. Pu, H. Guo, J. Chen, X. Wang, Y. Xi, C. Hu, Z.L. Wang, Eye motion triggered self-powered mechnosensational communication system using triboelectric nanogenerator, Sci. Adv. 3 (2017), e1700694.
[44] J. Luo, Z. Wang, L. Xu, A.C. Wang, K. Han, T. Jiang, Q. Lai, Y. Bai, W. Tang, F. R. Fan, Z.L. Wang, Flexible and durable wood-based triboelectric nanogenerators for self-powered sensing in athletic big data analytics, Nat. Commun. 10 (2019) 5147.
[45] X. Rong, J. Zhao, H. Guo, G. Zhen, J. Yu, C. Zhang, G. Dong, Material recognition sensor array by electrostatic induction and triboelectric effects, Adv. Mater. Technol. (2020), 2000641.
[46] S. Chen, Y. Pang, Y. Cao, X. Tan, C. Cao, Soft robotic manipulation system capable of stiffness variation and dexterous operation for safe human–machine interactions, Adv. Mater. Technol. 6 (2021), 2100084.